

Enhanced photoresponsivity in graphene-silicon slow-light photonic crystal waveguides

Hao Zhou, Tingyi Gu, James F. McMillan, Mingbin Yu, Guoqiang Lo, Dim-Lee Kwong, Guoying Feng, Shouhuan Zhou, and Chee Wei Wong

Citation: [Applied Physics Letters](#) **108**, 111106 (2016); doi: 10.1063/1.4944414

View online: <http://dx.doi.org/10.1063/1.4944414>

View Table of Contents: <http://scitation.aip.org/content/aip/journal/apl/108/11?ver=pdfcov>

Published by the [AIP Publishing](#)

Articles you may be interested in

[Enhanced four-wave mixing in graphene-silicon slow-light photonic crystal waveguides](#)

Appl. Phys. Lett. **105**, 091111 (2014); 10.1063/1.4894830

[Photonic crystal tunable slow light device integrated with multi-heaters](#)

Appl. Phys. Lett. **100**, 221110 (2012); 10.1063/1.4724191

[Electro-optic polymer infiltrated silicon photonic crystal slot waveguide modulator with 23 dB slow light enhancement](#)

Appl. Phys. Lett. **97**, 093304 (2010); 10.1063/1.3486225

[Solution-processed cavity and slow-light quantum electrodynamics in near-infrared silicon photonic crystals](#)

Appl. Phys. Lett. **95**, 131112 (2009); 10.1063/1.3238555

[APL Photonics](#)

A promotional banner for Applied Physics Reviews. On the left is a small image of a journal cover titled 'AIP Applied Physics Reviews' featuring a diagram of a photonic crystal. The main text reads 'NEW Special Topic Sections' in large white letters. Below this, it says 'NOW ONLINE' in yellow, followed by 'Lithium Niobate Properties and Applications: Reviews of Emerging Trends' in white. The AIP Applied Physics Reviews logo is in the bottom right corner.

NEW Special Topic Sections

NOW ONLINE
Lithium Niobate Properties and Applications:
Reviews of Emerging Trends

AIP Applied Physics
Reviews

Enhanced photoresponsivity in graphene-silicon slow-light photonic crystal waveguides

Hao Zhou,^{1,2,a)} Tingyi Gu,^{2,a)} James F. McMillan,² Mingbin Yu,³ Guoqiang Lo,³ Dim-Lee Kwong,³ Guoying Feng,¹ Shouhuan Zhou,¹ and Chee Wei Wong^{2,4,a)}

¹College of Electronics and Information Engineering, Sichuan University, Chengdu 610065, China

²Optical Nanostructures Laboratory, Columbia University, New York, New York 10027, USA

³Institute of Microelectronics, Singapore, Singapore 117685

⁴Mesoscopic Optics and Quantum Electronics Laboratory, University of California, Los Angeles, California 90095, USA

(Received 6 January 2016; accepted 5 March 2016; published online 17 March 2016)

We demonstrate the enhanced fast photoresponsivity in graphene hybrid structures by combining the ultrafast dynamics of graphene with improved light-matter interactions in slow-light photonic crystal waveguides. With a 200 μm interaction length, a 0.8 mA/W photoresponsivity is achieved in a graphene-silicon Schottky-like photodetector, with an operating bandwidth in excess of 5 GHz and wavelength range at least from 1480 nm to 1580 nm. Fourfold enhancement of the photocurrent is observed in the slow light region, compared to the wavelength far from the photonic crystal band-edge, for a chip-scale broadband fast photodetector. © 2016 AIP Publishing LLC.

[<http://dx.doi.org/10.1063/1.4944414>]

The optical bandwidth of solid-state group IV and III-V photodetectors is bounded by the semiconductor material band gap, and is typically weak for photon energy below the band gap or longer wavelengths. Concurrently, the intrinsic temporal photoresponse bandwidth is determined by the carrier mobilities and recombination timescales, with or without external applied bias electric fields. The unique optoelectronic properties of graphene, such as wavelength-independent absorption, remarkably high carrier mobility ($\approx 200\,000\text{ cm}^2\text{ v}^{-1}\text{ s}^{-1}$) in a single atomic layer crystal, which make it a potential material platform for high performance optoelectronic devices,^{1–8} including ultrafast photodetectors. A photodetector based on graphene is demonstrated for the high bandwidth 40 GHz operation, with a photoresponsivity of 0.5 to 6.1 mA/W.^{9,10} The structures of graphene photodetectors on chip are mainly graphene transistors on substrate and suspended, graphene p - n and p - i - n junctions, along with graphene on nanowires and graphene/silicon heterostructure waveguides.^{11–17} The main mechanisms such as the photovoltaic and photo-thermoelectric effects in these devices were recently reviewed in Ref. 18.

Although a single layer graphene absorbs only 2.3% of light, the photodetection efficiency has been significantly enhanced by waveguide integration or structural resonance such as Fabry-Pérot and photonic crystal microcavities or plasmon resonances in the visible wavelengths.^{19–23} The photoresponsivity has been enhanced to a very high level through the introduction of electron trapping centers, band gap engineering in high-purity monolayer graphene, and integrating an energy filtering barrier.^{24,25} Remarkably, a photoresponsivity as high as 10^7 A/W is obtained in graphene phototransistors with colloidal quantum dot films or graphene/MoS₂ heterostructures.^{26,27} The photoexcited ultrafast dynamics is also investigated experimentally. Dynamical

response times down to 2.1 ps and bandwidths up to ≈ 262 GHz are obtained in metal-graphene-metal photodetectors along with other approaches.^{17,28–30} Here we experimentally demonstrate a graphene Schottky-like photodetector integrated on a slow-light photonic crystal waveguide (PhCWG). Aided by the broadband absorption of graphene, large carrier mobility, as well as the slow-light enhanced light-matter interaction of the graphene-silicon hybrid structure, we achieve ≈ 4 times higher photoresponsivity enhancement compared to the region without slow light enhancement, based on the group index. We observed an operating bandwidth in excess of 5 GHz, covering the wavelength from 1480 nm to 1580 nm, and a photoresponsivity of 0.8 mA/W.

Fig. 1(a) shows the schematic of the graphene PhCWG. The line-defect PhCWG is fabricated on a doped silicon-on-insulator (SOI) wafer with deep ultraviolet lithography followed by reactive ion etching and buffered hydrofluoric wet etch, forming a 200 μm long air-bridged waveguide with an effective cross-sectional mode area about $0.55\ \mu\text{m}^2$. Chemical vapor deposited single layer graphene is wet-transferred onto the PhCWG, coupling to the PhCWG evanescent field. A Schottky barrier is formed at the graphene-silicon interface when the single layer graphene is contacted with the p -type region and n -type region of the silicon substrate, as shown in Figs. 1(a) and 1(c).^{31–34} The corresponding energy-band diagrams are shown in Fig. 1(b). The diagram on the left side of Fig. 1(b) is the energy-band diagram of graphene p -type-silicon junction at thermal equilibrium; the right one shows the energy-band diagram when graphene contact with the n -type silicon under reverse bias. E_F is the Fermi level, $\Phi_{\text{bp}}/\Phi_{\text{bn}}$ is the Schottky barrier of graphene p -type/ n -type junction, and V_{bias} is the bias voltage. The excited photon energy is around 0.8 eV (1550 nm), which is smaller than the band gap of silicon. Photons absorbed by graphene layer excited electron transitions directly from valence band to conduction band, generating electron-hole pairs.³⁴ When

^{a)}Authors to whom correspondence should be addressed. Electronic addresses: zhoufirst@scu.edu.cn; tg2342@columbia.edu; and cheewei.wong@ucla.edu

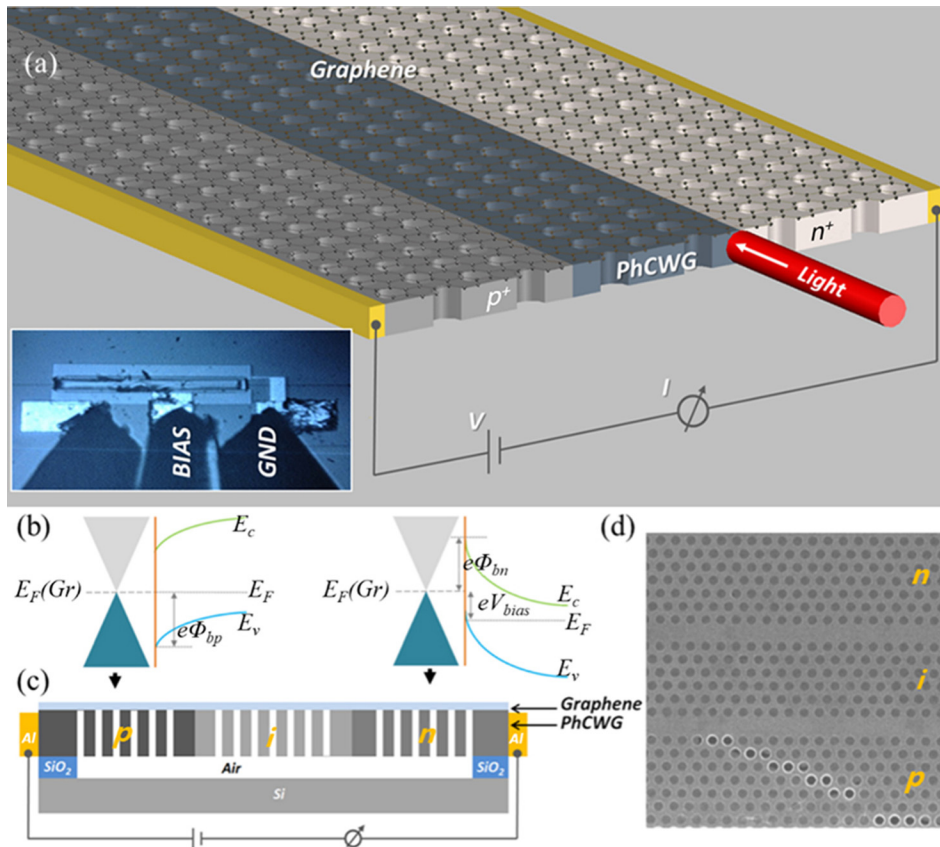


FIG. 1. Structure and band diagram of the device. (a) Structure schematic of the graphene-PhCWG photodetector. Inset: infrared image of the device with contacted probes. (b) Energy band diagram of the two different doping regions of the device. The left and the right panels, respectively, show the band diagrams without/with the bias voltages. (c) Cross-section schematic of air-bridged photonic crystal membrane with p - i - n regions contacted by top monolayer graphene. (d) Scanning electron micrograph (SEM) of device, with the gray (blurred) region covered by monolayer graphene while the white circles (focused) indicate the discontinuous regions without graphene.

the photon energy is higher than the Schottky barrier, the photogenerated carriers vertically pass through the graphene layer and is absorbed by Si, forming the photocurrent.³¹ The mechanism of graphene-silicon Schottky diode has been discussed in detail in Refs. 31–34; here, we mainly focus on the slow-light enhanced photoresponsivity in graphene-PhCWG.

Fig. 1(d) is the scanning electron microscopy (SEM) of a fabricated device, with two single line-defect PhCWGs, or two graphene-Schottky-like detectors in series. The coverage of the graphene on the PhCWG can be seen in Fig. 1(d). The waveguide is well covered by monolayer graphene, including the p - and n -doped area, enabling the current conduction and the interaction between graphene layer and evanescent field. The few photonic crystal holes with the bright white edges are not covered by graphene, due to the discontinuous regions of graphene during transfer. The photoresponsivity affected by these small regions is negligible. Fig. 2(a) shows the transmission of the graphene-PhCWG measured with amplified spontaneous emission (ASE) light source and optical spectrum analyzer. The group indices are measured by phase-delay method with fit shown by the orange dashed curve,³⁵ increasing from 12 to about 65 from 1530 nm to 1562 nm. Simultaneously, the transmission of the graphene-PhCWG decreases by about 30 dB.

The photocurrent of our photodetector is examined by using an ASE light source (Thorlabs ASE-FL7002 from 1530 nm to 1610 nm), a tunable continuous-wave (CW) laser (Ando AQ4321 from 1480 nm to 1580 nm), and mode-locked pulse fiber lasers with 39.1 MHz and 5 GHz repetition rates, pulse widths ≈ 3 ps, and 1550 nm center wavelength. The photocurrent is measured with a sensitive ampere meter

(Agilent 34401 A), and the DC bias voltages are applied via aluminum electrodes contacted to the p^+ area with conductive micro-probes [inset in Fig. 1(a)], and grounded at n^+ area. All measurements are performed at room temperature under ambient conditions.

Fig. 2(b) shows the photocurrent response under the continuous-wave ASE excitation. We test the photoresponse as a function of bias voltage when injecting ASE light. The incident light is injected by a lensed fiber (coupling loss ≈ 3 dB) located on the right side of the chip. Then, the light is coupled into the detector through a silicon coupler connected to the detector, with a coupled power into the waveguide at about 2.5 mW. The red filled and black open squares show the respective photocurrent and dark currents as a function of bias voltages. The current starts to arise around +0.5 V bias and increases quickly. The inset figure shows the current on a logarithmic scale. As the silicon detector can work when the energy of incident light below the band gap because of surface state absorption,³⁶ control experiment is performed without graphene. We emphasize that no photocurrent response is detected when we inject the ASE light into the same waveguide *before* graphene transfer, due to the sensitivity limitation of the ampere meter. While photocurrent response clearly observed after graphene transfer confirms that the responses we observed are from graphene-PhCWG hybrid structure, not from the silicon PhCWG.

Next, with the input power fixed at 2.5 mW, we measure the responsivity as a function of input wavelengths as shown in Figs. 3(a) and 3(b), for -4 V and $+1$ V bias voltages. Tunable laser light is used in this case. In both cases, we observe that the photoresponsivity increases when the input

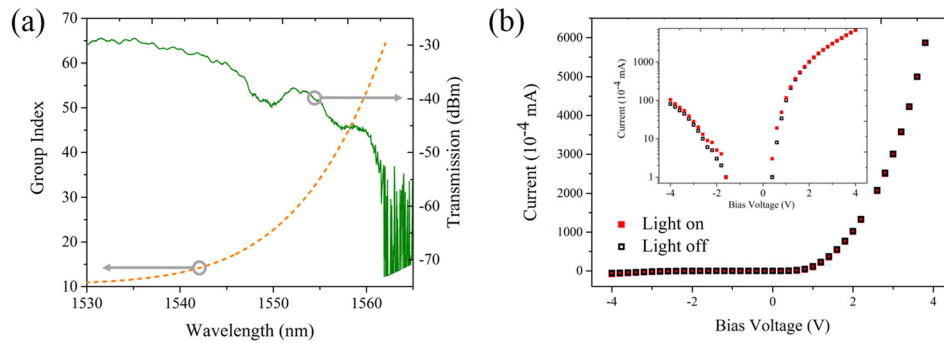


FIG. 2. Graphene-silicon photonic crystal waveguide optical transmission, group index and photocurrent responses. (a) Photonic crystal waveguide optical transmission spectrum (green curve) and the fitted group index dispersion (orange dashed curve). The optical absorption increases with increasing group index, at the slow-light propagation. (b) Measured photocurrent (red filled squares) and dark current (black open squares) under different bias voltages. Continuous-wave input light is used. The inset shows the logarithmic plot.

wavelength is tuned from 1480 nm to 1580 nm, and reaches its maximum value of ≈ 0.8 mA/W at around 1562 nm. This corresponds to the wavelength in which the highest group index is measurable. Then, the responsivity decreases when the wavelength continues to longer wavelength since the light is scattered when the laser wavelength is outside the transmission band. As the slow light effect enhances the light-matter interaction, the group index scaling of the absorption can be defined as $\alpha' = \alpha_{Gr} \frac{n_g}{n_0}$, where α_{Gr} is the absorption efficiency of graphene. The electron-hole pair production rate can be defined as $G = \Phi_0 \alpha' \exp(-\alpha' L)$,³⁷ where Φ_0 is the incoming photon flux and L is the propagation length. Hence, the higher group index results in higher photo response. The change of the responsivity matches the group index wavelength scaling, indicating the increasing group index enhances the absorption of the graphene layer. Fig. 3(c) plots the responsivity as a function of input power at 1 V bias voltage. The slope of the two data sequences shows the responsivity at 1530 nm and 1560 nm input wavelength is about 0.20 mA/W and 0.36 mA/W, respectively.

The wavelength band close to the higher group index has a higher slope, further verifying that the response is enhanced by slow-light effect. The step-like increment in Fig. 3(c) arises from the discretization of the current meter. The responsivity located at high group index band (1560 nm, $n_g = 55$) is about 2 times higher than the responsivity located at low group index band (1530 nm, $n_g = 12$). Compare to an even lower group index band around 1480 nm, the responsivity is increased by about 4 times with the slow-light enhanced light-matter interactions, which is also shown in Fig. 3(b).

The temporal dynamical response of the graphene-PhCWG is measured by a frequency spectrum analyzer (Anritsu, MS2721A), as shown in Fig. 4. We inject mode-locked fiber laser pulses (repetition rate 39.1 MHz, pulse width ≈ 3 ps, average power ≈ 2.5 mW, and wavelength at 1550 nm) into the device, and monitor the response as a function of bias voltages. We test the fast response under 5 GHz repetition rate pulses injection. The response peak is clear and sharp at about -95 dBm, which is about 10 dB

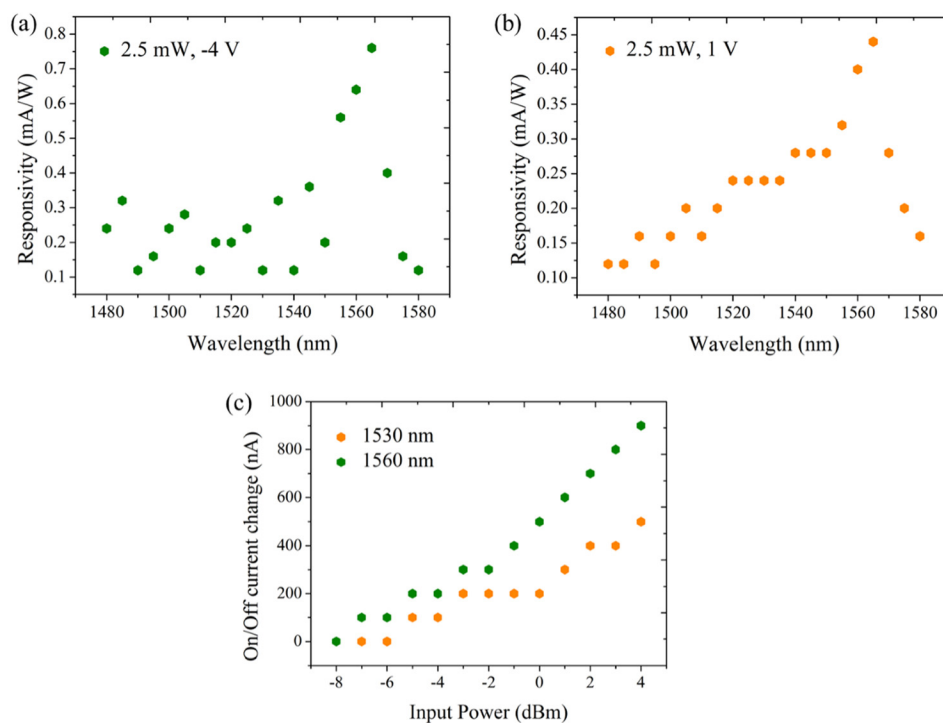


FIG. 3. Photoresponsivity as a function of wavelength and continuous-wave laser input power. (a) and (b) Photoresponsivity as a function of wavelength under the bias voltages of -4 V and $+1$ V, respectively. The photoresponsivity peaks at 1562 nm, corresponding to the high group index band measured. (c) Photoresponsivity as a function of input power when injecting 1530 nm (orange circles) and 1560 nm (green circles) laser light into the device, at 1 V bias voltage. The response is logarithmic with the input power, and the higher slope indicates higher responsivity. At 1530 nm and 1560 nm, the photoresponsivity is determined to be about 0.20 mA/W and 0.36 mA/W, respectively.

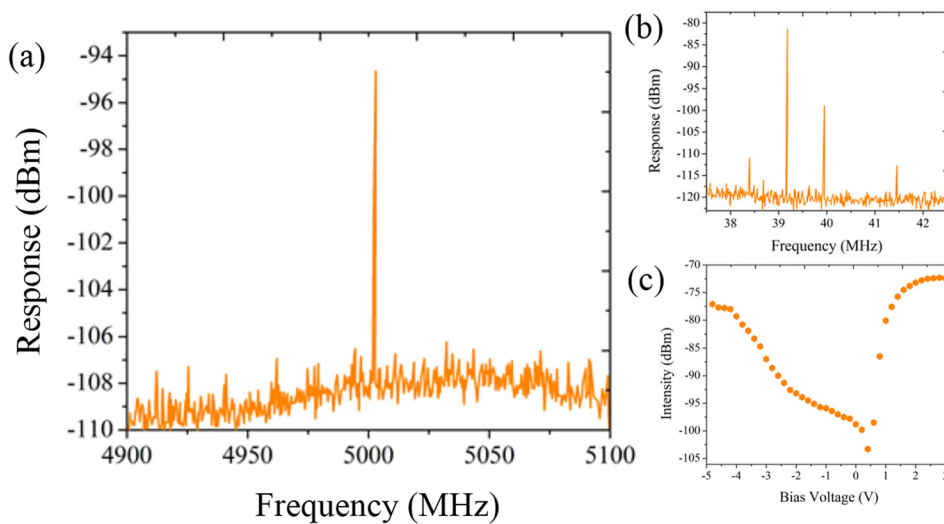


FIG. 4. Temporal dynamical response of the graphene-PhCWG device under different bias voltages. (a) Frequency responses of 5 GHz picosecond mode-locked fiber laser, under -4 V bias voltage. (b) Frequency responses under -4 V bias voltage and (c) photoresponsivity as a function of bias voltage, stimulated by 39.1 MHz picosecond mode-locked fiber laser. Small peaks in (b) are low frequency noises.

lower than 39.1 MHz pulse laser injection, as shown in Fig. 4(b), the other lower peaks are caused by low frequency noise. Figs. 4(a) and 4(b) indicate the detector has a better performance at lower frequency range. Compare the signal level to noise level, we could deduce that the detector has a detectivity of about -9 dBm (at 5 GHz) and -35 dBm (at 39.1 MHz). Limited by the repetition rate of the mode-locked laser and the spectrum range of the frequency analyzer, we did not measure higher repetition rates but prove our graphene-PhCWG device can act with at least 5 GHz detection. When increasing or reversing bias voltage, the response goes up from -105 dBm to about -72 dBm, and then reaches the highest level around $+3$ V and -4 V, as shown in Fig. 4(c). This result matches the responsivity versus bias voltage curves in Fig. 2(b). For present structure, the slow light effect will slow down the operation speed. There will be photocurrent when the incident light travels along the waveguide, and the current will last longer if the light goes slowly in the waveguide, equivalently slow down the operation speed.

In conclusion, in this work, we demonstrate a fourfold enhancement of the photoresponsivity in a slow-light graphene-silicon PhCWG on-chip. Compared to single-pass or graphene channel waveguide structures, the absorption efficiency is increased as the slow-light effect enhances the interaction between evanescent light field and graphene atomic layer. Measured photoresponses are observed from 1480 nm to 1580 nm band, with at least 5 GHz dynamical bandwidth achieved in our graphene-silicon device. The highest responsivity of about 0.8 mA/W is observed at the highest group index band around 1562 nm. The performance could be further improved by optimizing graphene coverage and multi-layer graphene transfer and the tradeoff between operation bandwidth and responsivity. The slow-light graphene-silicon device here demonstrates a feasible way to enhance the photoresponsivity, suggesting an alternative architecture in chip-integrated fast photodetectors.

The authors acknowledge helpful discussions from Shu-Wei Huang, Guoliang Deng, and support from the ONR program on nonlinear dynamics (N000141410041), the National Science Foundation IGERT (DGE-1069240), and the Chinese Scholarship Council.

- ¹A. K. Geim and K. S. Novoselov, *Nat. Mater.* **6**, 183 (2007).
- ²R. R. Nair, P. Blake, A. N. Grigorenko, K. S. Novoselov, T. J. Booth, T. Stauber, N. M. R. Peres, and A. K. Geim, *Science* **320**, 1308 (2008).
- ³J. M. Dawlaty, S. Shivaraman, J. Strait, P. George, M. Chandrashekar, F. Rana, M. G. Spencer, D. Veksler, and Y. Chen, *Appl. Phys. Lett.* **93**, 131905 (2008).
- ⁴F. Bonaccorso, Z. Sun, T. Hasan, and A. Ferrari, *Nat. Photonics* **4**, 611 (2010).
- ⁵K. I. Bolotin, K. J. Sikes, Z. Jiang, M. Klima, G. Fudenberg, J. Hone, P. Kim, and H. L. Stormer, *Solid State Commun.* **146**, 351 (2008).
- ⁶T. Gu, N. Petrone, J. McMillan, A. van der Zande, M. Yu, G. Q. Lo, D. L. Kwong, J. Hone, and C. W. Wong, *Nat. Photonics* **6**, 554 (2012).
- ⁷H. Zhou, T. Gu, J. F. McMillan, N. Petrone, A. van der Zande, J. Hone, M. Yu, G. Q. Lo, D. L. Kwong, G. Feng, S. Zhou, and C. W. Wong, *Appl. Phys. Lett.* **105**, 091111 (2014).
- ⁸Q. Bao, H. Zhang, Y. Wang, Z. Ni, Y. Yan, Z. X. Shen, K. P. Loh, and D. Y. Tang, *Adv. Funct. Mater.* **19**, 3077 (2009).
- ⁹F. Xia, T. Mueller, Y.-M. Lin, A. Valdes-Garcia, and P. Avouris, *Nat. Nanotechnol.* **4**, 839 (2009).
- ¹⁰T. Mueller, F. Xia, and P. Avouris, *Nat. Photonics* **4**, 297 (2010).
- ¹¹F. Xia, T. Mueller, R. Golizadeh-Mojarad, M. Freitag, Y.-M. Lin, J. Tsang, V. Perebeinos, and P. Avouris, *Nano Lett.* **9**, 1039 (2009).
- ¹²V. Patil, A. Capone, S. Strauf, and E.-H. Yang, *Sci. Rep.* **3**, 2791 (2013).
- ¹³V. Ryzhii, M. Ryzhii, V. Mitin, and T. Otsuji, *J. Appl. Phys.* **107**, 054512 (2010).
- ¹⁴N. M. Gabor, J. C. W. Song, Q. Ma, N. L. Nair, T. Taychatanapat, K. Watanabe, T. Taniguchi, L. S. Levitov, and P. Jarillo-Herrero, *Science* **334**, 648 (2011).
- ¹⁵A. V. Babichev, H. Zhang, P. Lavenus, F. H. Julien, A. Yu. Egorov, Y. T. Lin, L. W. Tu, and M. Tchernycheva, *Appl. Phys. Lett.* **103**, 201103 (2013).
- ¹⁶X. Gan, R.-J. Shiue, Y. Gao, I. Meric, T. F. Heinz, K. Shepard, J. Hone, S. Assefa, and D. Englund, *Nat. Photonics* **7**, 883 (2013).
- ¹⁷D. Schall, D. Neumaier, M. Mohsin, B. Chmielak, J. Bolten, C. Porschatis, A. Prinzen, C. Matheisen, W. Kuebart, B. Junginger, and W. Tempel, *ACS Photonics* **1**, 781 (2014).
- ¹⁸F. H. L. Koppens, T. Mueller, P. Avouris, A. C. Ferrari, M. S. Vitiello, and M. Polini, *Nat. Nanotechnol.* **9**, 780 (2014).
- ¹⁹M. Engel, M. Steiner, A. Lombardo, A. C. Ferrari, H. v. Löhneysen, P. Avouris, and R. Krupke, *Nat. Commun.* **3**, 906 (2012).
- ²⁰M. Furchi, A. Urich, A. Pospischil, G. Lilley, K. Unterrainer, H. Detz, P. Klang, A. M. Andrews, W. Schrenk, G. Strasser, and T. Mueller, *Nano Lett.* **12**, 2773 (2012).
- ²¹R.-J. Shiue, X. Gan, Y. Gao, L. Li, X. Yao, A. Szep, D. Walker, Jr., J. Hone, and D. Englund, *Appl. Phys. Lett.* **103**, 241109 (2013).
- ²²A. Ferreira, N. M. R. Peres, R. M. Ribeiro, and T. Stauber, *Phys. Rev. B* **85**, 115438 (2012).
- ²³Y. Liu, R. Cheng, L. Liao, H. Zhou, J. Bai, G. Liu, L. Liu, Y. Huang, and X. Duan, *Nat. Commun.* **2**, 579 (2011).
- ²⁴Y. Zhang, T. Liu, B. Meng, X. Li, G. Liang, X. Hu, and Q. J. Wang, *Nat. Commun.* **4**, 1811 (2013).
- ²⁵Y.-P. Hsieh, C. H. Yen, P. S. Lin, S. W. Ma, C. C. Ting, C. I. Wu, and M. Hofmann, *Appl. Phys. Lett.* **104**, 041110 (2014).
- ²⁶W. Zhang, C. P. Chuu, J. K. Huang, C. H. Chen, M. L. Tsai, Y. H. Chang, C. T. Liang, Y. Z. Chen, Y. L. Chueh, J. H. He, M. Y. Chou, and L. J. Li, *Sci. Rep.* **4**, 3826 (2014).

- ²⁷G. Konstantatos, M. Badioli, L. Gaudreau, J. Osmond, M. Bernechea, F. P. G. de Arquer, F. Gatti, and F. H. L. Koppens, *Nat. Nanotechnol.* **7**, 363 (2012).
- ²⁸A. Urich, K. Unterrainer, and T. Mueller, *Nano Lett.* **11**, 2804 (2011).
- ²⁹D. Sun, G. Aivazian, A. M. Jones, J. S. Ross, W. Yao, D. Cobden, and X. Xu, *Nat. Nanotechnol.* **7**, 114 (2012).
- ³⁰A. Pospischil, M. Humer, M. M. Furchi, D. Bachmann, R. Guider, T. Fromherz, and T. Mueller, *Nat. Photonics* **7**, 892 (2013).
- ³¹M. Amirmazlaghani, F. Raissi, O. Habibpour, J. Vukusic, and J. Stake, *IEEE J. Quantum Electron.* **49**, 589 (2013).
- ³²C. C. Chen, M. Aykol, C. C. Chang, A. F. J. Levi, and S. B. Cronin, *Nano Lett.* **11**, 1863 (2011).
- ³³X. An, F. Liu, Y. J. Jung, and S. Kar, *Nano Lett.* **13**, 909 (2013).
- ³⁴X. Wang, Z. Cheng, K. Xu, H. K. Tsang, and J.-B. Xu, *Nat. Photonics* **7**, 888 (2013).
- ³⁵J. F. McMillan, M. Yu, D. L. Kwong, and C. W. Wong, *Opt. Express* **18**, 15484 (2010).
- ³⁶T. Baehr-Jones, M. Hochberg, and A. Scherer, *Opt. Express* **16**, 1659 (2008).
- ³⁷S. M. Sze and K. K. Ng, *Physics of Semiconductor Devices*, 3rd ed. (John Wiley & Sons, 2006).